EurJIC
European Journal of Inorganic Chemistry

Research Article
doi.org/10.1002/ejic.202100905

Chemistry Europe
European Chemical Societies Publishing

www.eurjic.org

Protic Ferrocenyl Acyclic Diamino Carbene Gold(I) Complexes

Sven D. Waniek,[a] Christoph Förster,*[a] and Katja Heinze*[a]

Dedicated to the memory of Prof. Dr. Gottfried Huttner

Two mononuclear protic ferrocenyl acyclic diamino carbene gold(I) complexes AuCl[C(NHFc)(NR_2)] were prepared by nucleophilic attack of diethylamine (R = Et) and diisopropylamine (R = ^{i}Pr) at the ferrocenyl substituted isocyanide complex chlorido (isocyanoferrocene)gold(I) AuCl(CN–Fc). In the solid state, the multifunctional protic carbene gold(I) complexes display intermolecular aurophilic interactions or intermolecular NH···Cl hydrogen bonding in addition to intramolecular non-classical NH···Fe hydrogen bonds. Oxidation of the AuCl[C(NHFc)(NR_2)] complexes initially takes place at the iron centres giving highly coloured ferrocenium ions, which subsequently likely undergo electron transfer from gold(I) to iron(III) yielding putative EPR-active gold(II) species.

Introduction

The multifaceted coordination chemistry[1,2] of gold makes gold complexes play a vital role in catalysis[3–6] in their typical oxidation states +I[7–9] and +III.[10] In gold(I) catalysis, typically precatalysts of the type AuCl(L) are employed with phosphanes or carbenes as ligands L (Scheme 1), well suited to stabilise the reactive cationic species $[Au(L)]^+$.[7,9] Beside N-heterocyclic carbenes in gold catalysis,[11,12] cyclic amino alkyl carbenes (CAAC)[13] and acyclic diamino carbenes (ADC)[14–19] with their stronger donicity and differing steric bulk[20,21] have demonstrated to be promising candidates. Complexes Au(CAAC)Cl enable new catalytic applications, e.g. the direct hydroamination of alkynes or allenes with hydrazine.[22] The gold(I) catalysed addition of indole to 1,6-enynes yields the cyclopropane product with AuCl(NHC) as pre-catalyst, while Au(ADC)Cl with similar steric bulk shows a different selectivity, giving the alkene as main product.[19] Gold(I) complexes with hydrogen-bond supported heterocyclic carbenes (HBHC), ADCs with intramolecular hydrogen bonding (Scheme 1),[18,23,24] can also show differences in selectivity to their NHC counterparts, e.g. in the cyclization of 1,6-enynes with the *endo* form as preferred product, while the *exo* product is obtained from the NHC complex.[24] Gold(I) complexes with ADC ligands are acessible from gold(I) isonitriles with primary or secondary amines.[16–18,25–28] These ADCs with N(H)R substituents can be viewed as protic ADCs, similar to protic NHCs,[29–31] which are also decribed as ligands in gold complexes.[32–35]

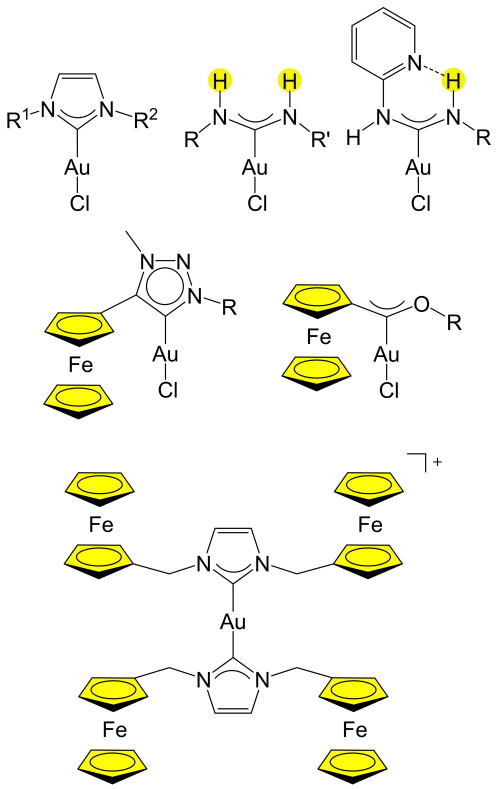

Scheme 1. Schematic representation of gold(I) complexes with N-heterocyclic carbene (NHC), protic acyclic diamino carbene ligands (ADC), hydrogen bond supported heterocyclic carbene (HBHC) (top), ferrocenyl substituted mesoionic carbene, Fischer carbene and NHC ligands (center/bottom).

[a] S. D. Waniek, Dr. C. Förster, Prof. Dr. K. Heinze
Department of Chemistry
Johannes Gutenberg University of Mainz
Duesbergweg 10–14, 55128 Mainz, Germany
E-mail: cfoerster@uni-mainz.de
katja.heinze@uni-mainz.de
www.ak-heinze.chemie.uni-mainz.de

Supporting information for this article is available on the WWW under https://doi.org/10.1002/ejic.202100905

Part of the https://chemistry-europe.onlinelibrary.wiley.com/doi/toc/10.1002/(ISSN)1099-0682c. Ferrocene-Chemistry Ferrocene Chemistry Special Collection.

Research Article
doi.org/10.1002/ejic.202100905

Commonly, the use of activators, halide scavengers like silver(I) salts, fascilitating the dissociation of the chlorido ligand from AuCl(L) are necessesary to form the active catalyst $[Au(L)]^+$. Also silver-free activation by e.g. in situ replacing the chlorido ligand using alkali metal salts, copper(II) triflate or methyl triflate is possible.[36–40] Alternatively, introducing ferrocenyl (Fc) as redox-active moiety in carbene[41–44] (Scheme 1) or phosphane ligands[45] and oxidizing the ferrocene to ferrocenium can initiate catalysis. The reversible on/off switching of the catalyst leads to redox-switchable gold catalysis. Recently, the combination of redox- and proton-switchable moieties in a gold(I) complex has been reported.[46] Ferrocenyl substituted carbenes, typically NHCs,[47,48] mesoionic carbenes[42–44,49–51] and Fischer-type carbenes[41,52] have been coordinated to gold(I). To the best of our knowledge, gold(I) complexes with ferrocenyl substituted ADCs have not been reported up to now.

One-electron oxidation of the Fischer-type ferrocenyl carbene complex AuCl[C(OEt)Fc] to $\{AuCl[C(OEt)Fc]\}^+$ has been suggested to yield a mononuclear gold(II) complex as catalytically competent species.[41] Beside the EPR spectroscopic detection of the final Fe^{II}/Au^{II} valence isomer, the postulated initially formed intermediate Fe^{III}/Au^{I} species could not been detected in this case. However, counter ion and solvent dependent $Au^{III}(porph^{\bullet-})\rightarrow Au^{II}(porph)$ valence isomerization equilibria have been observed for porphyrinato gold complexes ($porph^{2-}$ = substituted porphyrinato(2-)).[53–55]

Here we combine protic ADCs with redox-active ferrocenyl substituents coordinated to gold(I). We describe the synthesis of protic ferrocenyl ADC gold(I) complexes starting from an isocyanoferrocene gold(I) complex, their solid state structures and their redox properties using cyclic voltammetry, square wave voltammetry, chemical oxidation followed by UV/Vis/NIR and X-band EPR spectroscopy and density functional theory (DFT) calculations. We discuss the potential electron transfer chain in the cationic ADC gold complexes, prepared by chemical oxidation, as monitored by UV/Vis/NIR and X-band EPR spectroscopy.

Results and Discussion

Synthesis and Characterization

Addition of secondary amines to isocyanide gold(I) complexes yields the corresponding protic acyclic diamino carbene gold(I) complexes.[16–18,25–28] To install the redox-active ferrocene unit, we first coordinated isocyanoferrocene Fc–NC[56] to gold(I) chloride via chlorido(dimethylsulfide)gold(I) as gold(I) precursor giving the heterobimetallic complex chlorido (isocyanoferrocene)gold(I) **1** in 27% isolated yield (Scheme 2). The conceivable inverse route to the envisioned ADC gold(I) complexes starting from an (alkylisocyano) chlorido gold(I) complex and aminoferrocene was unsuccessful due to the low nucleophilicity of aminoferrocene.[57,58]

While the reaction of 1,1′-diisocyanoferrocene and chlorido (dimethylsulfide) gold(I) affords an insoluble coordination polymer with aurophilic interactions,[59] the mono(isocyano)

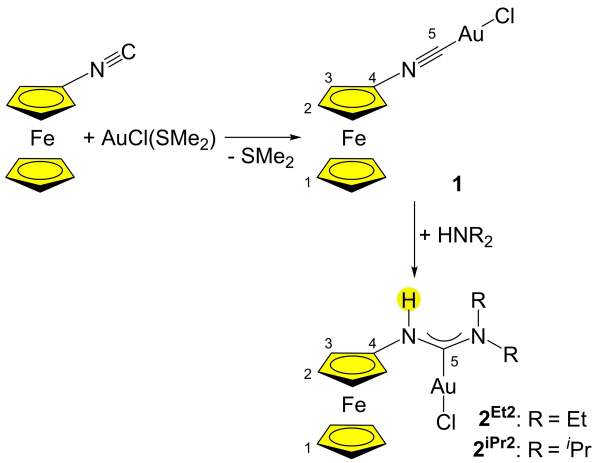

Scheme 2. Synthesis of isocyanoferrocene complex **1** and protic ferrocenyl acyclic diamino carbene complexes $\mathbf{2^{Et2}}$ and $\mathbf{2^{iPr2}}$. Atom numbering for NMR assignments indicated. Ferrocenyl substituents and NH proton highlighted in yellow.

complex **1** is well soluble in common organic solvents. **1** is characterized by its CN stretching vibration at 2225 cm^{-1} (Supporting Information, Figure S1) shifted by 101 cm^{-1} to higher energy as compared to Fc–NC (2124 cm^{-1})[56] and similar to the shift difference of the pair AuCl(4-CN-C_6H_4OMe)/4-CN-C_6H_4OMe (2123/2221 cm^{-1}).[17] The ^{1}H NMR spectrum of **1** displays the expected three resonances in a 2:5:2 ratio for the ferrocenyl substituent (Supporting Information, Figure S2). The ^{13}C NMR resonance of the coordinated isocyanide in **1** in CD_2Cl_2 is observed at δ = 164.7 ppm as a triplet with $^1J_{NC}$ = 5.7 Hz due to coupling to ^{14}N (Supporting Information, Figure S3), slightly shifted to lower field as compared to that of Fc–NC with δ = 163.9 ppm (t, 5.6 Hz).[56] The $APCI^+$ mass spectrum of **1** indicates facile dissociation of chloride and coordination of CH_3CN (m/z = 449, Supporting Information, Figure S4).

ADC gold(I) complexes $\mathbf{2^{Et2}}$ and $\mathbf{2^{iPr2}}$ were formed by nucleophilic attack of the secondary amines $HNEt_2$ and $HN(^iPr_2)$ at the isocyanide complex **1** in 67% and 55% isolated yields, respectively (Scheme 2). Expectedly, the IR band for the CN stretching vibration of **1** has vanished in the carbene complexes $\mathbf{2^{Et2}}$ and $\mathbf{2^{iPr2}}$ (Supporting Information, Figures S5–S6). The NH stretching vibration of the protic diaminocarbene ligands in $\mathbf{2^{Et2}}$ and $\mathbf{2^{iPr2}}$ appear in the ATR IR spectra at 3270 and 3268 cm^{-1}, respectively. The ^{1}H NMR resonances of the NH units turn up at 7.03 and 7.20 ppm in CD_2Cl_2, respectively (Supporting Information, Figures S7–S8). The ^{13}C NMR resonances of the gold coordinated carbon atoms shift to δ = 190.5 and 191.6 ppm in $\mathbf{2^{Et2}}$ and $\mathbf{2^{iPr2}}$, respectively (Supporting Information, Figures S9-S11), a range expected for coordinated diaminocarbenes, e.g. δ = 190.0 ppm was found for chlorido[(diethylamino)(4-methoxyphenylamino) methylidene]gold(I).[17] The chlorido ligand easily dissociates in ESI^+ mass spectra of $\mathbf{2^{Et2}}$ and $\mathbf{2^{iPr2}}$ (m/z = 481 and 509, respectively) and is partially replaced by a solvent molecule CH_3CN (m/z = 522 and 550, respectively) or another intact gold(I) complex (m/z = 997 and 1053, respectively),

Research Article
doi.org/10.1002/ejic.202100905

presumably forming a bridging chlorido ligand (Supporting Information, Figures S12–S13).[60]

Structure Determination

Single crystals of $\mathbf{2}^{Et2}$ and $\mathbf{2}^{iPr2}$ suitable for X-ray diffraction analyses were obtained by recrystallization from THF/petroleum ether. While both complexes display the expected linear coordination at the gold(I) ion, a *syn* conformation and unremarkable bond lengths and angles around the gold and ferrocene units (Supporting Information, Table S1), the packing in the crystalline state strongly differs (Figure 1). In principle, several intermolecular interactions are conceivable in these multifunctional complexes, namely classical NH···Cl hydrogen bonding, non-classical NH···Fe hydrogen bonding[58,61,62] and aurophilic interactions.[63–65] The ethyl derivative $\mathbf{2}^{Et2}$ displays a NH···Cl hydrogen bonding motif with a N···Cl distance of 3.402(4) Å giving chains of complexes along the crystallographic *b* axis (Figure 1a). This motif is similar to NH···O/S hydrogen bonds of ferrocenyl amides, ferrocenyl thioamides, ferrocenyl ureas and ferrocenyl (thio)ureas in the solid state.[66–68] On the other hand, isopropyl derivative $\mathbf{2}^{iPr2}$ realizes aurophilic interactions with an Au···Au distance of 3.1897(3) Å in a centrosymmetric dimer (Figure 1b), while chlorido diaminocarbene gold(I) complexes with dialkylamino and arylamino substituents display no aurophilic interactions[17] except of chloride [(diethylamino)(pyridylamino)methylidene] gold(I) forming a dimer with an Au···Au distance of 3.3107(14) Å.[23] The observed Au···Au distance of $\mathbf{2}^{iPr2}$ in the solid state correlates to a bond dissociation energy $D_e = 12.7 \times 10^6\ e^{-3.5d(Au-Au)} = 18\ kJ\,mol^{-1}$ (*d* in Å, D_e in $kJ\,mol^{-1}$) according to an equation derived by Schwerdtfeger.[69,70]

In addition to the intermolecular NH···Cl hydrogen bonding ($\mathbf{2}^{Et2}$) or aurophilic interaction in the centrosymmetric dimer ($\mathbf{2}^{iPr2}$), the iron centers of the ferrocene units in $\mathbf{2}^{Et2}$ and $\mathbf{2}^{iPr2}$ engage in weak intramolecular non-classical NH···Fe hydrogen bonds with N···Fe distances of 3.0760(34) Å and 3.0629(27) Å, respectively (Figure 1).[58,61,62] The strong non-classical NH···Fe hydrogen bond with an N···Fe distance of 3.46 Å in a ferrocenyl hydrazone exhibits a dissociation energy of 13 $kJ\,mol^{-1}$.[61] Clearly, the energetics of the observed intra- and intermolecular interactions of the protic ferrocenyl acyclic diamino carbene gold(I) complexes $\mathbf{2}^{Et2}$ and $\mathbf{2}^{iPr2}$ – hydrogen bonding and aurophilicity – are of similar magnitude.

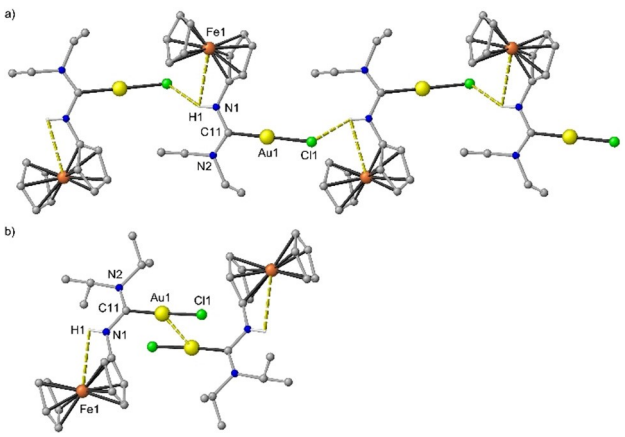

Figure 1. Molecular structures and intermolecular interactions of a) $\mathbf{2}^{Et2}$ and b) $\mathbf{2}^{iPr2}$ in the crystal as determined by X-ray diffraction.

Redox and Optical Properties

Fc–NC is oxidized to $[Fc–NC]^+$ at 350 mV vs. ferrocene[71] while the redox potential of the isocyano gold(I) complex pair $[\mathbf{1}]^+/\mathbf{1}$ amounts to $E_{1/2} = 540$ mV (Supporting Information, Figures S14–S15). On the other hand, the diaminocarbene complexes $\mathbf{2}^{Et2}$ and $\mathbf{2}^{iPr2}$ are oxidized reversibly to $[\mathbf{2}^{Et2}]^+$ and $[\mathbf{2}^{iPr2}]^+$ at 105 and 115 mV vs. ferrocene in $CH_2Cl_2/[^nBu_4N][B(C_6F_5)_4]$, respectively (Supporting Information, Figures S16–S19). These values are lower by 440–475 mV compared to that of the $[\mathbf{1}]^+/\mathbf{1}$ and chlorido (ferrocenyl Fischer carbene) gold(I) redox couples,[41] but at typical potentials of N-substituted ferrocenes,[68] N-ferrocenyl amides, thioamides,[72] ureas, thioureas[73] or chlorido Fc-MIC gold(I) complexes.[44]

Consequently, the oxidation process is assigned to the ferrocene/ferrocenium redox couple, rather than an $Au^{II/I}$ couple.[41,55,74–76] Geometry optimizations of the $\mathbf{2}^{Et2}/[\mathbf{2}^{Et2}]^+$ and $\mathbf{2}^{iPr2}/[\mathbf{2}^{iPr2}]^+$ redox pairs on the DFT level of theory (CPCM (CH_2Cl_2)-(U)B3LYP-D3BJ/def2-TZVPP) corroborate this assignment based on Fe–C distances and Mulliken spin densities at the metal ions (Supporting Information, Tables S2–S5). In both complexes $[\mathbf{2}^{Et2}]^+$ and $[\mathbf{2}^{iPr2}]^+$, the Mulliken spin densities at the iron and gold centers amount to 1.25 and 0.00, respectively, suggesting a negligible spin delocalization onto the gold center. This spin localization at the iron centers fits to the low $Fe^{III/II}$ redox potential precluding any gold(II) contribution.

The UV/Vis/NIR spectra of the yellow complexes **1**, $\mathbf{2}^{Et2}$ and $\mathbf{2}^{iPr2}$ in CH_2Cl_2 display the characteristic ferrocene bands at 434, 439 and 438 nm, respectively (Supporting Information, Figures S20–S22). Although many carbene gold(I) complexes can be luminescent,[23] ferrocene typically quenches luminescence, either via energy transfer or via electron transfer.[77,78] Expectedly, both ferrocenyl complexes $\mathbf{2}^{Et2}$ and $\mathbf{2}^{iPr2}$ are non-emissive at room temperature and at 77 K with excitation at 254 nm.

The cations $[\mathbf{2}^{Et2}]^+$ and $[\mathbf{2}^{iPr2}]^+$, prepared by chemical oxidation with one equivalent of $[N(4\text{-}C_6H_4Br)_3][SbCl_6]$ (magic blue, $E_{1/2} = 700$ mV vs. ferrocene in CH_2Cl_2)[79] in THF are strongly colored with absorption bands at 573/759 and 535/759 nm, respectively (Figure 2). These weakly solvatochromic bands (Experimental Section, Supporting Information Figures S23, S24) are tentatively assigned to transitions with nitrogen lone pairs to iron(III) charge transfer character according to time-dependent DFT (TDDFT) calculations and analyses of the electron density difference maps (Supporting Information, Figures S25–S28). The higher energy transition in $[\mathbf{2}^{iPr2}]^+$ possesses some additional $[Au^I–Cl]$ to iron(III) character, while the analogous transitions in $[\mathbf{2}^{Et2}]^+$ are of negligibly small oscillator strength. The rather poor agreement of TDDFT calculated spectra with

Research Article
doi.org/10.1002/ejic.202100905

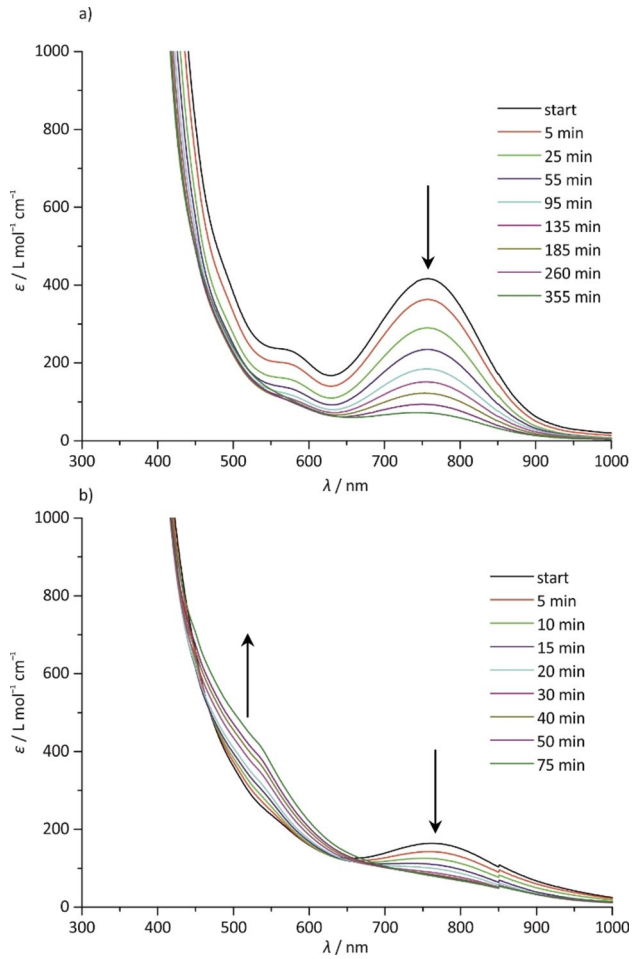

Figure 2. UV/Vis/NIR spectra in THF of a) $[\mathbf{2}^{Et2}]^+$ prepared by oxidation with $[N(4\text{-}C_6H_4Br)_3][SbCl_6]$ from $\mathbf{2}^{Et2}$ and b) $[\mathbf{2}^{iPr2}]^+$ prepared by oxidation with $[N(4\text{-}C_6H_4Br)_3][SbCl_6]$ from $\mathbf{2}^{iPr2}$ over time.

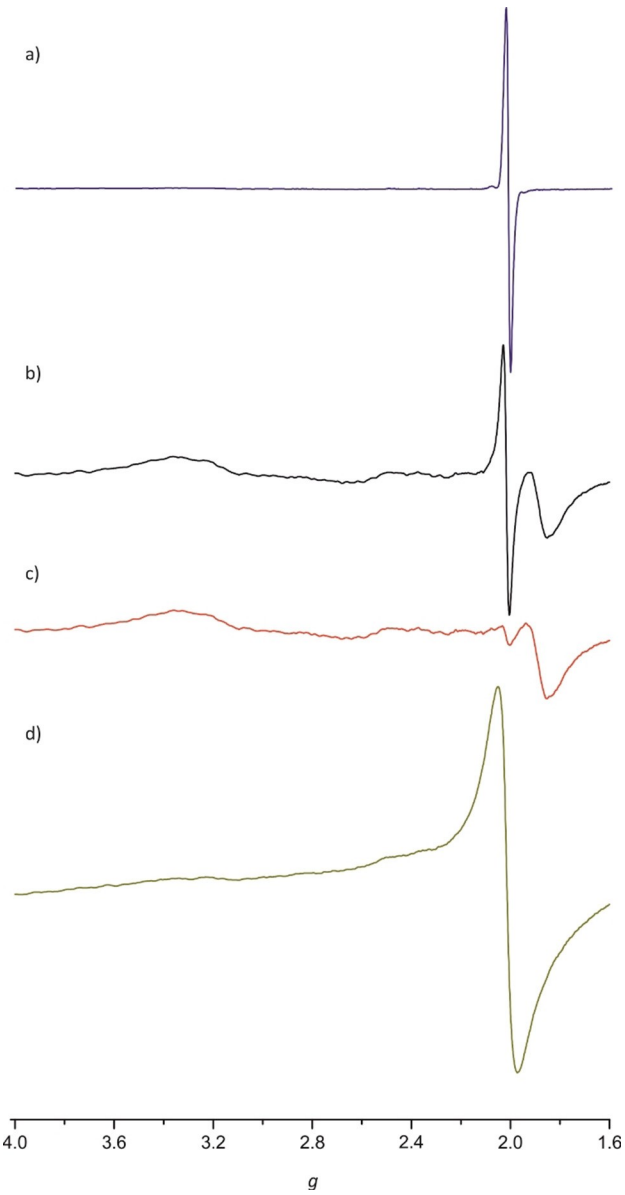

Figure 3. X-band EPR spectra of a) magic blue $[N(4\text{-}C_6H_4Br)_3][SbCl_6]$, b) a mixture of $\mathbf{2}^{iPr2}$ with one equivalent of magic blue rapidly frozen, c) after storing the mixture for 30 min. at 195 K and d) followed by storing the mixture at 295 K for 3.5 h. All spectra were recorded in THF at 77 K.

experimental spectra of metallocenes has been noted before, allowing only a qualitative description.[80,81]

Both cationic complexes are stable on the time scale of the voltammetric experiments. However, $[\mathbf{2}^{Et2}]^+$ and $[\mathbf{2}^{iPr2}]^+$ further react on the time scale of hours after chemical oxidation (Figure 2). Several possibilities can be suggested, namely deprotonation at the amine after oxidation of the ferrocene,[82,83] slow electron transfer from gold(I) to iron(III)[41] followed by dimerization of the gold(II) radical,[84,85] formation of gold(III) via disproportionation or chlorine radical/Cl_2 formation followed by oxidative addition,[86–89] or chloride loss from gold(I)[60] followed by chloride attack on iron(III) of the multifunctional open-shell complexes $[\mathbf{2}^{Et2}]^+$ and $[\mathbf{2}^{iPr2}]^+$.

To experimentally confirm the thermodynamically and kinetically feasible initial oxidation of the iron(II) center, pre-cooled solutions of $\mathbf{2}^{Et2}$ and $\mathbf{2}^{iPr2}$ with one equivalent of magic blue ($[N(4\text{-}C_6H_4Br)_3][SbCl_6]$) in THF were rapidly frozen to 77 K and X-band EPR spectra were recorded (Figure 3, Supporting Information Figure S29). Besides the resonance of residual magic blue at $g \approx 2.016$ (Figure 3a), resonances at $g \approx 3.36$ and $g \approx 1.89$ (inflexion point), typical for the low- and high-field tensor components of N-substituted ferrocenium ions are observed (Figure 3b; Supporting Information Figures S29b).[82,83] Upon warming to 195 K, the resonance of magic blue decreases rapidly in intensity, while the ferrocenium resonance persists (Figure 3c, Supporting Information Figure S29c). Further warming to room temperature results in the appearance of a new very broad resonance at $g \approx 2.014$ and in disappearing of the ferrocenium resonances (Figure 3d, Supporting Information Figure S29d). The broad resonance is similar to the Au^{II} resonance with unresolved hyperfine coupling to the gold nucleus (^{197}Au: $I = {}^3/_2$) at $g_{iso} = 2.017$ observed for the species formed from the cationic ferrocenyl Fischer-type gold complex {AuCl[C(Fc)OEt]}$^+$.[41] Hence, we assign these final broad resonances to gold

(II)-centered radical species after oxidation of $\mathbf{2}^{Et2}$ and $\mathbf{2}^{iPr2}$, which could form via an $Fe^{III}/Au^{I} \rightarrow Fe^{II}/Au^{II}$ intramolecular electron transfer (IET) after the initial Fc/Fc^{+} oxidation. Unfortunately, the exact nature of the final species after oxidation of $\mathbf{2}^{Et2}$ and $\mathbf{2}^{iPr2}$ observed by EPR spectroscopy remains unclear. The EPR resonances of these species are even observable at room temperature and increase over time at room temperature (Supporting Information, Figures S30-S31), reaching a maximum intensity after ca. 23 h. Concomitantly, the characteristic UV/Vis/NIR absorption bands of the ferrocenium complexes $[\mathbf{2}^{Et2}]^{+}$ and $[\mathbf{2}^{iPr2}]^{+}$ at 759 nm decrease in intensity at room temperature (Figure 2). The decay of the Fc^{+} absorption bands and the parallel rise of the putative gold(II) EPR resonances (Supporting Information, Figure S32) give spectroscopic evidence of the $Fe^{III}/Au^{I} \rightarrow Fe^{II}/Au^{II}$ IET in $[\mathbf{2}^{Et2}]^{+}$ and $[\mathbf{2}^{iPr2}]^{+}$ or in respective follow-up products. The EPR active species from the reaction of the closely related carbene gold(I) complex AuCl[C(Fc)OEt] with magic blue formed with 75% yield obtained almost quantitatively, supporting the $Fe^{III}/Au^{I} \rightarrow Fe^{II}/Au^{II}$ IET.[41] The rather slow electron transfer from gold(I) to iron(III) likely occurs with small reorganization at the iron center but with large structural reorganization at the gold ion. For example, $[SbCl_6]^{-}$ anion and/or solvent could coordinate to the gold ion under expansion of the coordination sphere from linear for gold(I) to square planar for gold(II),[74] stabilizing the Fe^{II}/Au^{II} species.[41] The absence of a well resolved ^{197}Au hyperfine coupling pattern may be due to spin delocalization over the gold(II) bonded ligands, as calculated for $Au^{II}Cl$[C-(Fc)OEt]$(SbCl_6)$.[41] Alternatively, spin exchange interactions of distant Au^{II} centers in oligonuclear aggregates could be responsible as observed for mononuclear gold(II) complex compounds in the solid.[74b]

While the Fc/Fc^{+} oxidation is more facile in $\mathbf{2}^{Et2}/\mathbf{2}^{iPr2}$ than in the Fischer carbene complex AuCl[C(Fc)OEt][41] and with the assumption that the redox potentials for the Au^{I}/Au^{II} oxidation are rather similar for all these gold(I) complexes, the driving force for the proposed IET might be lower in the ADC complexes $\mathbf{2}^{Et2}/\mathbf{2}^{iPr2}$. This lower driving force should increase the electron transfer barrier for the IET in $\mathbf{2}^{Et2}/\mathbf{2}^{iPr2}$, which allows the spectroscopic detection of the ferrocenium valence isomers of $[\mathbf{2}^{Et2}]^{+}$ and $[\mathbf{2}^{iPr2}]^{+}$ before formation of the putative gold(II) species.

The redox chemistry of AuCl[C(Fc)OEt][41] and the ADC gold (I) complexes $\mathbf{2}^{Et2}$ and $\mathbf{2}^{iPr2}$ makes these complexes potential candidates as pre-catalysts without the necessity for halide abstraction for activation but oxidative activation instead, e.g. in catalyzed phenol synthesis, hydration of alkynes,[17] methoxycyclization of 1,6-enynes[18] or cyclisation of *N*(2-propyn-1-yl) benzamide.[41–44] Catalysis experiments with $\mathbf{2}^{Et2}$, $\mathbf{2}^{iPr2}$ and derivatives as pre-catalysts under oxidative conditions and redox-switchable catalysis will be addressed in future studies.

Conclusion

Protic ferrocenyl acyclic diamino carbene gold(I) complexes have been prepared from chlorido(isocyanoferrocene)gold(I) and secondary amines NHR_2 (R = Et, ^{i}Pr). The complexes were characterized structurally and spectroscopically. The multifunctionality enables various structural motifs in the solid state, namely NH···Cl and NH···Fe hydrogen bonds as well as aurophilic interactions. Reversible oxidation to the respective cations is feasible on the time scale of cyclic and square wave voltammetry. The initial formation of ferrocenium ions was verified EPR spectroscopically for the first time. Slow follow-up, possibly intramolecular, electron transfer yields persistent EPR-active species, likely with gold(II) character. Their potential in redox-switchable gold catalysis will be exploited in the future.

Experimental Section

Reactions and measurements were performed under argon atmosphere unless otherwise noted using Gloveboxes (*UniLab/MBraun* – Ar 4.8, $O_2 < 1$ ppm, $H_2O < 0.1$ ppm) or Schlenk techniques. Dichloromethane and acetonitrile were dried and distilled from calcium hydride. THF and petroleum ether were dried and distilled from potassium and sodium, respectively. Dry methanol was purchased from *Acros Organics*. Deuterated solvents were purchased from *Deutero GmbH*. Other reagents were used as received from commercial suppliers (*Strem Chemicals*, *Apollo Scientific* and *Acros Organics*). Fc–NC was prepared according to a literature method.[56]

Crystal Structure Determinations. Data for $\mathbf{2}^{Et2}$ were collected with an *IPDS 2T* single crystal x-ray diffractometer from *STOE & CIE GmbH* and corrected for absorption and other effects using Mo K_α radiation ($\lambda = 0.71073$ Å). The diffraction frames were integrated using the *STOE X-Area* software package,[90] and most were corrected for absorption with *MULABS*[91] of the *PLATON* software package.[92] Crystal structure data for $\mathbf{2}^{iPr2}$ were collected with a *STADIVARI* diffractometer from *STOE & CIE GmbH* using Mo K_α radiation ($\lambda = 0.71073$ Å). The diffraction frames were integrated using the *STOE X-Area* software package[90] and were corrected for absorption with *STOE LANA*.[93] The structures were solved by direct methods and refined by the full-matrix method based on F^2 using the *SHELX* software package[94–96] and the *ShelXle* graphical interface.[97] All non-hydrogen atoms were refined anisotropically, while the position of hydrogen atoms were generated with appropriate geometric constraints and allowed to ride on their respective parent atoms with fixed isotropic thermal parameters.

Crystallographic Data of $\mathbf{2}^{Et2}\times$THF. $C_{15}H_{20}AuClFeN_2\times$THF (588.70); monoclinic; $P2_1/n$; $a = 9.2897(19)$ Å, $b = 14.204(3)$ Å, $c = 15.637(3)$ Å, $\beta = 98.66(3)^\circ$; $V = 2039.8(7)$ Å^3; $Z = 4$; density, calcd. = 1.917 g cm^{-3}, $T = 120(2)$ K, $\mu = 8.035$ mm^{-1}; F(000) = 1144; crystal size 0.160 × 0.110 × 0.050 mm; $\theta = 2.403$ to 27.891 deg.; $-10 \le h \le 12$, $-16 \le k \le 18$, $-20 \le l \le 20$; rfln collected = 12268; rfln unique = 4853 [R(int) = 0.0411]; completeness to $\theta = 25.242$ deg. = 99.8%; semi empirical absorption correction from equivalents; max. and min. transmission 1.30375 and 0.77806; data 4853; restraints 0, parameters 228; goodness-of-fit on $F^2 = 1.061$; final indices [$I > 2\sigma(I)$] $R_1 = 0.0278$, w$R_2 = 0.0612$; R indices (all data) $R_1 = 0.0373$, w$R_2 = 0.0653$; largest diff. peak and hole 0.765 and −0.889 e Å^{-3}.

Crystallographic Data of $\mathbf{2}^{iPr2}$. $C_{17}H_{24}AuClFeN_2$ (544.65); triclinic; $P\bar{1}$; $a = 7.7203(3)$ Å, $b = 9.8414(3)$ Å, $c = 12.5908(4)$ Å, $\alpha = 69.153(3)^\circ$; $\beta = 79.014(3)^\circ$; $\gamma = 83.656(4)^\circ$; $V = 876.67(5)$ Å^3; $Z = 2$; density, calcd. = 2.063 g cm^{-3}, $T = 120(2)$ K, $\mu = 9.335$ mm^{-1}; F(000) = 524; crystal size 0.200 × 0.138 × 0.075 mm; $\theta = 2.217$ to 30.734 deg.; $-10 \le h \le 10$, $-12 \le k \le 14$, $-17 \le l \le 17$; rfln collected = 12307; rfln unique = 4804 [R(int) = 0.0230]; completeness to $\theta = 25.242$ deg. = 100.0%; semi empirical absorption correction from equivalents; max. and min. transmission 0.4826 and 0.1426; data 4804; restraints 0, parameters 203; goodness-of-fit on $F^2 = 1.037$; final indices [$I > 2\sigma(I)$] $R_1 = 0.0263$,

$wR_2 = 0.0645$; R indices (all data) $R_1 = 0.0284$, $wR_2 = 0.0654$; largest diff. peak and hole 1.219 and -3.258 e Å^{-3}.

Density functional theory calculations were performed with Orca 4.1.1[98] using the high performance computing cluster *ELWE-TRITSCH*. The B3LYP[99–101] formulation of DFT and Def2-tzvpp[102,103] as basis set which uses polarization functions for non-hydrogen atoms were used. For solvent modelling keyword *CPCM*[104,105] in CH_2Cl_2 was applied. The "*zeroth order regular approximation*" (keyword *ZORA*)[106–108] was used for relativistic corrections. For the gold atom the segmented all-electron relativistically contracted (SARC) basis set (SARC-ZORA-TZVPP) by Pantazis et al. was employed.[106] The RIJCOSX[109–111] approximation was used to accelerate the calculations. Atom-pairwise dispersion correction was performed with the Becke-Johnson damping scheme (keyword D3BJ).[112,113] The energy of the electronic states and presence of energy minima were checked by numerical frequency calculations. Explicit counter ions and/or solvent molecules were not taken into account

NMR spectra were recorded on a *Bruker Avance DRX 400* spectrometer at 400 MHz (^{1}H) and 100 MHz (^{13}C) at 25 °C. All resonances are reported in ppm versus the solvent signal as internal standard: CD_2Cl_2 (^{1}H, $\delta = 5.32$; ^{13}C, $\delta = 54.24$ ppm).[114] **ESI and APCI mass spectra** were recorded with an *Agilent 6545 QTOF mass spectrometer*. **UV/Vis/NIR spectra** were recorded on a *Varian Cary 5000* or a *Jasco V770* spectrometer using 1.0 cm quartz cells with a Schott valve. **ATR IR spectra** were recorded on a Bruker ALPHA II FT-IR spectrometer with a Platinum Di-ATR module under ambient conditions. **Electrochemical experiments** were carried out on a *BioLogic SP-200* voltammetric analyzer using platinum wires as counter and working electrodes and 0.01 M $Ag/AgNO_3$ as the reference electrode. The measurements were carried out at a scan rate of 100 mV s^{-1} for cyclic voltammetry experiments and at 50 mV s^{-1} for square-wave voltammetry experiments using $[^nBu_4N][B(C_6F_5)_4]$ as the supporting electrolyte in CH_2Cl_2. Potentials are referenced to the ferrocene/ferrocenium couple by using ferrocene as a standard for the isocyano complex **1** ($E_{1/2} = 260$ mV under the experimental conditions) and decamethylferrocene as a standard for the carbene complexes **2** ($E_{1/2} = -590$ mV under the experimental conditions). **X-band EPR spectra** were recorded on a *Miniscope MS 300* (Magnettech GmbH, Germany) with a frequency counter *FC 400* (Magnettech GmbH, Germany) or *HewlettPackard 5340A* at a microwave frequency of 9.39 GHz at room temperature or 77 K, Mn^{2+} in ZnS was used as external standard ($g = 2.118$, 2.066, 2.027, 1.986, 1.946, 1.906). **Elemental analyses** were performed by the central analytic service of the department of chemistry of the University of Mainz with an *Vario El cube* from *Elementar*.

Synthesis of AuCl(CN-Fc) 1 [similar to a literature procedure for (1′-(diphenylphosphino)-1-isocyanoferrocene)$(AuCl)_2$].[115,116] 200 mg (0.68 mmol, 1 eq) of chlorido(dimethyl sulfide)gold(I) was dissolved in CH_2Cl_2 (15 mL). Isocyanoferrocene (143.3 mg, 0.68 mmol, 1 eq) was added as solid and the solution was stirred for 10–15 minutes. The solvent was removed under reduced pressure. Recrystallization from THF/petroleum ether yielded **1** as yellow powder in 27% yield (81 mg, 0.18 mmol). Elemental analysis calcd. (%) for $C_{11}H_9ClFeAuN$ (443.64) + 0.25 C_4H_7O (THF): C 31.25, H 2.35, N 3.04; found C 31.05, H 2.50, N 3.19. ^{1}H NMR (400.31 MHz, CD_2Cl_2): $\delta = 4.81$ (pt, 2H, H^3), 4.40 (s, 5 H, H^1), 4.35 (pt, 2 H, H^2) ppm. ^{13}C{^{1}H} NMR (100.66 MHz, CD_2Cl_2): $\delta = 164.7$ (t, C^5, $^1J_{NC} = 5.7$ Hz), 79.3 (t, C^4, $^1J_{NC} = 15.8$ Hz), 71.2 (C^1), 67.4 (C^2), 67.3 (C^3) ppm. MS (APCI, CH_3CN): m/z (%) = 449.00 (100), 450.00 (16), 451.01 (2) [**1**-Cl + CH_3CN]$^+$. IR (ATR): $\tilde{\nu} = 3099$ (w, CH), 2225 (s, C≡N), 1409 (m), 1240 (w), 1104 (m), 1023 (m), 999 (m), 923 (m), 813 (s), 484 (vs) cm^{-1}. CV (CH_2Cl_2/$[^nBu_4N][B(C_6F_5)_4]$): $E_{1/2}$ = 540 mV vs. ferrocene/ferrocenium. UV/Vis/NIR (CH_2Cl_2): λ (ε/M^{-1} cm^{-1}) = 434 (430) nm.

Synthesis of 2^{Et2}. Chlorido(isocyanoferrocene) gold(I) **1** (133.0 mg, 0.30 mmol, 1 eq) was dissolved in CH_2Cl_2 (25 mL). Diethylamine (0.15 mL, 1.50 mmol, 5 eq, 109.7 mg) was added under exclusion of light and the solution was stirred for one hour at room temperature. The solvent was removed under reduced pressure. Recrystallization from THF/petroleum ether yielded **2^{Et2}** as yellow crystals in 67% yield (104 mg, 0.20 mmol). Elemental analysis calcd. (%) for $C_{15}H_{20}ClFeAuN_2$ (516.60 g mol^{-1}): C 34.88, H 3.90, N 5.42; found C 34.76, H 4.01, N 5.45. ^{1}H NMR (400.31 MHz, CD_2Cl_2): $\delta = 7.03$ (s, 1 H, NH), 4.71 (pt, 2 H, H^3), 4.26 (s, 5 H, H^1), 4.13 (pt, 2 H, H^2), 3.98 (q, $^3J_{HH} = 7.1$ Hz, 2 H, CH_2), 3.42 (q, 2 H, $^3J_{HH} = 7.3$ Hz, CH_2), 1.31 (m, 6 H, CH_3) ppm. ^{13}C{^{1}H} NMR (100.66 MHz, CD_2Cl_2): $\delta = 190.5$ (C^5), 98.5 (C^2), 70.1 (C^1), 66.3 (C^4), 65.7 (C^3), 54.8 (CH_2), 41.9 (CH_2), 14.9 (CH_3), 12.7 (CH_3) ppm. MS (ESI$^+$, CH_3CN): m/z (%) = 481.06 (79), 482.07 (14), 483.07 (2) [**2^{Et2}**-Cl]$^+$, 520.09 (6), 521.09 (1), 522.09 (100), 523.09 (21), 524.09 (24) [**2^{Et2}**-Cl + CH_3CN]$^+$, 997.10 (10), 998.10 (4), 999.10 (4), 1000.10 (2) [(**2^{Et2}**-Cl)$_2$Cl]$^+$. IR (ATR): $\tilde{\nu} = 3270$ (w, NH), 2963 (w, CH), 1545 (vs), 1368 (s), 1139 (m), 1104 (s), 811 (m), 486 (vs) cm^{-1}. CV (CH_2Cl_2/$[^nBu_4N][B(C_6F_5)_4]$): $E_{1/2}$ = 105 mV vs. ferrocene/ferrocenium. UV/Vis/NIR (THF): λ (ε/M^{-1} cm^{-1}) = 435 (309) nm. UV/Vis/NIR (CH_2Cl_2): λ (ε/M^{-1} cm^{-1}) = 439 (210) nm. UV/Vis/NIR (CH_3CN): λ (ε/M^{-1} cm^{-1}) = 433 (255) nm.

Synthesis of 2^{iPr2}. Chlorido(isocyanoferrocene) gold(I) **1** (215.4 mg, 0.49 mmol, 1 eq) was dissolved in CH_2Cl_2 (25 mL). Diisopropylamine (0.34 mL, 2.43 mmol, 5 eq, 245.7 mg) was added under exclusion of light and the solution was stirred for one hour at room temperature. The solvent was removed under reduced pressure. Recrystallization from THF/petroleum ether yielded **2^{iPr2}** as yellow crystals in 55% yield (146 mg, 0.27 mmol). Elemental analysis calcd. (%) for $C_{17}H_{24}ClFeAuN_2$ (544.65 g mol^{-1}): C 37.49, H 4.44, N 5.14; found C 37.60, H 4.62, N 5.31. ^{1}H NMR (400.31 MHz, CD_2Cl_2): $\delta = 7.18$ (s, 1 H, NH), 4.65 (pt, 2 H, H^3), 4.25 (s, 5 H, H^1), 4.16 (pt, 2 H, H^2), 3.92 (m, 1 H, CH) 1.51 (d, 6 H, CH_3), 1.51–1.30 (m, 1 H, CH), 1.30 (d, 6 H, CH_3) ppm. ^{13}C{^{1}H} NMR (100.66 MHz, CD_2Cl_2): $\delta = 191.6$ (C^5), 98.1 (C^2), 69.8 (C^1), 66.5 (C^4), 62.4 (C^3), 46.8 (CH), 21.4 (CH_3), 21.0 (CH_3) ppm. MS (ESI$^+$, CH_3CN): m/z (%) = 509.10 (78), 510.10 (16), 511.10 (2) [**2^{iPr2}**–Cl]$^+$, 548.13 (6), 549.13 (1), 550.13 (100), 551.13 (23), 552.13 (3) [**2^{iPr2}**-Cl + CH_3CN]$^+$, 1053.16 (16), 1054.16 (7), 1055.16 (6), 1056.16 (2) [(**2^{iPr2}**-Cl)$_2$Cl]$^+$. IR (ATR): $\tilde{\nu} = 3268$ (w, NH), 2969 (w, CH), 1547 (vs), 1370 (s), 1139 (s), 1104 (m), 813 (m), 486 (vs) cm^{-1}. CV (CH_2Cl_2/$[^nBu_4N][B(C_6F_5)_4]$): $E_{1/2}$ = 115 mV vs. ferrocene/ferrocenium. UV/Vis/NIR (THF): λ (ε/M^{-1} cm^{-1}) = 432 (336) nm. UV/Vis/NIR (CH_2Cl_2): λ (ε/M^{-1} cm^{-1}) = 438 (220) nm. UV/Vis/NIR (CH_3CN): λ (ε/M^{-1} cm^{-1}) = 433 (256) nm.

Oxidation of 2^{Et2} and 2^{iPr2} – UV/Vis/NIR spectroscopic monitoring. The complexes (**2^{Et2}**: 1.49 mg, 0.0029 mmol; **2^{iPr2}**: 1.58 mg, 0.0029·mmol) were dissolved under inert atmosphere at room temperature in THF, CH_3CN, CH_2Cl_2 or CH_3OH (3 mL), respectively. A UV/Vis/NIR spectrum was recorded. The oxidant $[N(4\text{-}C_6H_4Br)_3][SbCl_6]$ (2.36 mg, 0.0029 mmol) was added as a solid and UV/Vis/NIR spectra were recorded after the indicated time intervals.

Oxidation of 2^{iPr2} – EPR spectroscopic monitoring. To pre-cooled (dry ice/ethanol) solutions of **2^{Et2}** or **2^{iPr2}** (1.72 mg/1.82 mg, 0.0033 mmol) in THF (0.5 mL) was added a solution of magic blue $[N(4\text{-}C_6H_4Br)_3][SbCl_6]$ (2.36 mg, 0.0029 mmol) in THF (0.3 mL) under inert atmosphere. The EPR tubes were immediately cooled to 77 K in the EPR spectrometer. Analogous experiments and spectroscopic monitoring were performed at room temperature under inert atmosphere. EPR spectra of magic blue (1.06 mg, 0.0013 mmol) in THF (0.5 mL) were recorded at room temperature and at 77 K for comparison.

Deposition Numbers 2107165 (for **2^{Et2}**×THF) and 2107164 (for **2^{iPr2}**) contain the supplementary crystallographic data for this paper. These data are provided free of charge by the joint Cambridge

Crystallographic Data Centre and Fachinformationszentrum Karlsruhe Access Structures service www.ccdc.cam.ac.uk/structures.

Acknowledgements

Financial support from the Deutsche Forschungsgemeinschaft HE 2778/16-1 is gratefully acknowledged. Parts of this research were conducted using the supercomputer ELWETRITSCH and advisory services offered by the Technical University of Kaiserslautern (https://elwe.rhrk.uni-kl.de/), which is a member of the AHRP. We thank Dr. Dieter Schollmeyer and Dr. Luca M. Carrella for collection of the diffraction data. Open Access funding enabled and organized by Projekt DEAL.

Conflict of Interest

The authors declare no conflict of interest.

Data Availability Statement

The data that support the findings of this study are available in the supplementary material of this article.

Keywords: Acyclic carbenes · Diamino carbenes · Ferrocene ligands · Gold · Redox properties

[1] R. P. Herrera, M. C. Gimeno, *Chem. Rev.* **2021**, *121*, 8311–8363.
[2] G. J. Hutchings, M. Brust, H. Schmidbaur, *Chem. Soc. Rev.* **2008**, *37*, 1759–1765.
[3] P. Font, X. Ribas, *Eur. J. Inorg. Chem.* **2021**, *2021*, 2556–2569.
[4] A. S. K. Hashmi, *Acc. Chem. Res.* **2014**, *47*, 864–876.
[5] A. S. K. Hashmi, *Angew. Chem. Int. Ed.* **2010**, *49*, 5232–5241; *Angew. Chem.* **2010**, *122*, 5360–5369.
[6] A. Fürstner, *Chem. Soc. Rev.* **2009**, *38*, 3208–3221.
[7] A. Collado, D. J. Nelson, S. P. Nolan, *Chem. Rev.* **2021**, *121*, 8559–8612.
[8] R. Dorel, A. M. Echavarren, *Chem. Rev.* **2015**, *115*, 9028–9072.
[9] C. Obradors, A. M. Echavarren, *Chem. Commun.* **2014**, *50*, 16–28.
[10] L. Rocchigiani, M. Bochmann, *Chem. Rev.* **2021**, *121*, 8364–8451.
[11] D. Gatineau, J.-P. Goddard, V. Mouriès-Mansuy, L. Fensterbank, *Isr. J. Chem.* **2013**, *53*, 892–900.
[12] N. Marion, S. P. Nolan, *Chem. Soc. Rev.* **2008**, *37*, 1776–1782.
[13] R. Jazzar, M. Soleilhavoup, G. Bertrand, *Chem. Rev.* **2020**, *120*, 4141–4168.
[14] L. M. Slaughter, *ACS Catal.* **2012**, *2*, 1802–1816.
[15] V. P. Boyarskiy, K. V. Luzyanin, V. Y. Kukushkin, *Coord. Chem. Rev.* **2012**, *256*, 2029–2056.
[16] A. A. Ruch, M. C. Ellison, J. K. Nguyen, F. Kong, S. Handa, V. N. Nesterov, L. M. Slaughter, *Organometallics* **2021**, *40*, 1416–1433.
[17] A. S. K. Hashmi, T. Hengst, C. Lothschütz, F. Rominger, *Adv. Synth. Catal.* **2010**, *352*, 1315–1337.
[18] C. Bartolomé, Z. Ramiro, D. García-Cuadrado, P. Pérez-Galán, M. Raducan, C. Bour, A. M. Echavarren, P. Espinet, *Organometallics* **2010**, *29*, 951–956.
[19] H. Seo, B. P. Roberts, K. A. Abboud, K. M. Merz, S. Hong, *Org. Lett.* **2010**, *12*, 4860–4863.
[20] C. Singh, A. Kumar, H. V. Huynh, *Inorg. Chem.* **2020**, *59*, 8451–8460.
[21] M. Soleilhavoup, G. Bertrand, *Acc. Chem. Res.* **2015**, *48*, 256–266.
[22] R. Kinjo, B. Donnadieu, G. Bertrand, *Angew. Chem. Int. Ed.* **2011**, *50*, 5560–5563; *Angew. Chem.* **2011**, *123*, 5674–5677.
[23] C. Bartolomé, M. Carrasco-Rando, S. Coco, C. Cordovilla, J. M. Martín-Alvarez, P. Espinet, *Inorg. Chem.* **2008**, *47*, 1616–1624.
[24] C. Bartolomé, Z. Ramiro, P. Pérez-Galán, C. Bour, M. Raducan, A. M. Echavarren, P. Espinet, *Inorg. Chem.* **2008**, *47*, 11391–11397.
[25] V. Vethacke, V. Claus, M. C. Dietl, D. Ehjeij, A. Meister, J. F. Huber, L. K. Paschai Darian, M. Rudolph, F. Rominger, A. S. K. Hashmi, *Adv. Synth. Catal.* **2021**, *363*, DOI: 10.1002/adsc.202101000.
[26] R. Usón, A. Laguna, J. Vicente, J. García, B. Bergareche, *J. Organomet. Chem.* **1979**, *173*, 349–355.
[27] J. E. Parks, A. L. Balch, *J. Organomet. Chem.* **1974**, *71*, 453–463.
[28] F. Bonati, G. Minghetti, *J. Organomet. Chem.* **1973**, *59*, 403–410.
[29] S. Kuwata, F. E. Hahn, *Chem. Rev.* **2018**, *118*, 9642–9677.
[30] M. C. Jahnke, F. E. Hahn, *Coord. Chem. Rev.* **2015**, *293–294*, 95–115.
[31] M. C. Jahnke, F. E. Hahn, *Chem. Lett.* **2015**, *44*, 226–237.
[32] J. Ruiz, M. A. Mateo, *Organometallics* **2021**, *40*, 1515–1522.
[33] J. Ruiz, L. García, D. Sol, M. Vivanco, *Angew. Chem. Int. Ed.* **2016**, *55*, 8386–8390; *Angew. Chem.* **2016**, *128*, 8526–8530.
[34] P. C. Kunz, C. Wetzel, S. Kögel, M. U. Kassack, B. Spingler, *Dalton Trans.* **2011**, *40*, 35–37.
[35] H. G. Raubenheimer, L. Lindeque, S. Cronje, *J. Organomet. Chem.* **1996**, *511*, 177–184.
[36] A. Franchino, M. Montesinos-Magraner, A. M. Echavarren, *Bull. Chem. Soc. Jpn.* **2021**, *94*, 1099–1117.
[37] R. Pretorius, M. R. Fructos, H. Müller-Bunz, R. A. Gossage, P. J. Pérez, M. Albrecht, *Dalton Trans.* **2016**, *45*, 14591–14602.
[38] L. Hettmanczyk, D. Schulze, L. Suntrup, B. Sarkar, *Organometallics* **2016**, *35*, 3828–3836.
[39] H. Schmidbaur, A. Schier, *Z. Naturforsch. B* **2011**, *66*, 329–350.
[40] S. Gaillard, J. Bosson, R. S. Ramón, P. Nun, A. M. Z. Slawin, S. P. Nolan, *Chem. Eur. J.* **2010**, *16*, 13729–13740.
[41] P. Veit, C. Volkert, C. Förster, V. Ksenofontov, S. Schlicher, M. Bauer, K. Heinze, *Chem. Commun.* **2019**, *55*, 4615–4618.
[42] S. Klenk, S. Rupf, L. Suntrup, M. van der Meer, B. Sarkar, *Organometallics* **2017**, *36*, 2026–2035.
[43] L. Hettmanczyk, L. Suntrup, S. Klenk, C. Hoyer, B. Sarkar, *Chem. Eur. J.* **2017**, *23*, 576–585.
[44] L. Hettmanczyk, S. Manck, C. Hoyer, S. Hohloch, B. Sarkar, *Chem. Commun.* **2015**, *51*, 10949–10952.
[45] A. Straube, P. Coburger, L. Dütsch, E. Hey-Hawkins, *Chem. Sci.* **2020**, *11*, 10657–10668.
[46] B. S. Birenheide, F. Krämer, L. Bayer, P. Mehlmann, F. Dielmann, F. Breher, *Chem. Eur. J.* **2021**, *27*, DOI: 10.1002/chem.202101969.
[47] J. F. Arambula, R. McCall, K. J. Sidoran, D. Magda, N. A. Mitchell, C. W. Bielawski, V. M. Lynch, J. L. Sessler, K. Arumugam, *Chem. Sci.* **2016**, *7*, 1245–1256.
[48] J. K. Muenzner, B. Biersack, A. Albrecht, T. Rehm, U. Lacher, W. Milius, A. Casini, J.-J. Zhang, I. Ott, V. Brabec, O. Stuchlikova, I. C. Andronache, L. Kaps, D. Schuppan, R. Schobert, *Chem. Eur. J.* **2016**, *22*, 18953–18962.
[49] C. Hoyer, P. Schwerk, L. Suntrup, J. Beerhues, M. Nössler, U. Albold, J. Dernedde, K. Tedin, B. Sarkar, *Eur. J. Inorg. Chem.* **2021**, *2021*, 1373–1382.
[50] K. Škoch, P. Vosáhlo, I. Císařová, P. Štěpnička, *Dalton Trans.* **2020**, *49*, 1011–1021.
[51] D. Aucamp, S. V. Kumar, D. C. Liles, M. A. Fernandes, L. Harmse, D. I. Bezuidenhout, *Dalton Trans.* **2018**, *47*, 16072–16081.
[52] D. I. Bezuidenhout, B. van der Westhuizen, A. J. Rosenthal, M. Wörle, D. C. Liles, I. Fernández, *Dalton Trans.* **2014**, *43*, 398–401.
[53] S. Preiß, J. Melomedov, A. Wünsche von Leupoldt, K. Heinze, *Chem. Sci.* **2016**, *7*, 596–610.
[54] Z. Ou, K. M. Kadish, W. E. J. Shao, P. J. Sintic, K. Ohkubo, S. Fukuzumi, M. J. Crossley, *Inorg. Chem.* **2004**, *43*, 2078–2086.
[55] K. Heinze, *Angew. Chem. Int. Ed.* **2017**, *56*, 16126–16134; *Angew. Chem.* **2017**, *129*, 16342–16350.
[56] G. R. Knox, P. L. Pauson, D. Willison, E. Solčániová, Š. Toma, *Organometallics* **1990**, *9*, 301–306.
[57] P. Veit, S. Seibert, C. Förster, K. Heinze, *Z. Anorg. Allg. Chem.* **2020**, *646*, 940–947.
[58] P. Veit, C. Förster, S. Seibert, K. Heinze, *Z. Anorg. Allg. Chem.* **2015**, *641*, 2083–2092.
[59] U. Siemeling, D. Rother, C. Bruhn, H. Fink, T. Weidner, F. Träger, A. Rothenberger, D. Fenske, A. Priebe, J. Maurer, R. Winter, *J. Am. Chem. Soc.* **2005**, *127*, 1102–1103.
[60] S. F. Hartlaub, N. K. Lauricella, C. N. Ryczek, A. G. Furneaux, J. D. Melton, N. A. Piro, W. S. Kassel, C. Nataro, *Eur. J. Inorg. Chem.* **2017**, *2017*, 424–432.

[61] C. Förster, P. Veit, V. Ksenofontov, K. Heinze, *Chem. Commun.* **2015**, *51*, 1514–1516.
[62] P. Veit, E. Prantl, C. Förster, K. Heinze, *Organometallics* **2016**, *35*, 249–257; in Druck.
[63] N. Mirzadeh, S. H. Privér, A. J. Blake, H. Schmidbaur, S. K. Bhargava, *Chem. Rev.* **2020**, *120*, 7551–7591.
[64] H. Schmidbaur, A. Schier, *Chem. Soc. Rev.* **2012**, *41*, 370–412.
[65] H. Schmidbaur, *Gold Bull.* **2000**, *33*, 3–10.
[66] D. Siebler, C. Förster, K. Heinze, *Dalton Trans.* **2011**, *40*, 3558–3575.
[67] D. Siebler, M. Linseis, T. Gasi, L. M. Carrella, R. F. Winter, C. Förster, K. Heinze, *Chem. Eur. J.* **2011**, *17*, 4540–4551.
[68] K. Heinze, M. Schlenker, *Eur. J. Inorg. Chem.* **2004**, 2974–2988.
[69] P. Pyykkö, *Angew. Chem. Int. Ed.* **2004**, *43*, 4412–4456; *Angew. Chem.* **2004**, *116*, 4512–4557.
[70] P. Schwerdtfeger, A. E. Bruce, M. R. M. Bruce, *J. Am. Chem. Soc.* **1998**, *120*, 6587–6597.
[71] T. El-Shihi, F. Siglmüller, R. Herrmann, M. Fernanda, N. N. Carvalho, A. J. Pombeiro, *J. Organomet. Chem.* **1987**, *335*, 239–247.
[72] T. Kienz, C. Förster, K. Heinze, *Organometallics* **2014**, *33*, 4803–4812.
[73] K. Hanauer, M. T. Pham, C. Förster, K. Heinze, *Eur. J. Inorg. Chem.* **2017**, *2017*, 433–445.
[74] a) S. Preiß, C. Förster, S. Otto, M. Bauer, P. Müller, D. Hinderberger, Haeri, Haleh, Hashemi, L. Carella, K. Heinze, *Nat. Chem.* **2017**, *9*, 1249–1255; b) R. Kirmse, M. Kampf, R.-M. Olk, M. Hildebrand, H. Krautscheid, *Z. Anorg. Allg. Chem.* **2004**, *630*, 1433–1436.
[75] T. Drews, S. Seidel, K. Seppelt, *Angew. Chem. Int. Ed.* **2002**, *41*, 454–456; *Angew. Chem.* **2002**, *114*, 470–473.
[76] A. J. Blake, J. A. Greig, A. J. Holder, T. I. Hyde, A. Taylor, M. Schröder, *Angew. Chem. Int. Ed. Engl.* **1990**, *29*, 197–198; *Angew. Chem.* **1990**, *102*, 203–204.
[77] S. Fery-Forgues, B. Delavaux-Nicot, *J. Photochem. Photobiol. A* **2000**, *132*, 137–159.
[78] J. Melomedov, J. R. Ochsmann, M. Meister, F. Laquai, K. Heinze, *Eur. J. Inorg. Chem.* **2014**, *2014*, 2902–2915.
[79] N. G. Connelly, W. E. Geiger, *Chem. Rev.* **1996**, *96*, 877–910.
[80] S. D. Waniek, J. Klett, C. Förster, K. Heinze, *Beilstein J. Org. Chem.* **2018**, *14*, 1004–1015.
[81] M. Yáñez-S, S. A. Moya, C. Zúñiga, G. Cárdenas-Jirón, *Comput. Theor. Chem.* **2017**, *1118*, 65–74.
[82] A. Neidlinger, T. Kienz, K. Heinze, *Organometallics* **2015**, *34*, 5310–5320.
[83] A. Neidlinger, V. Ksenofontov, K. Heinze, *Organometallics* **2013**, *32*, 5955–5965.
[84] J. Holz, M. Ayerbe García, W. Frey, F. Krupp, R. Peters, *Dalton Trans.* **2018**, *47*, 3880–3905.
[85] M. R. Ringenberg, J. Holz, R. Peters, *Dalton Trans.* **2018**, *47*, 12873–12878.
[86] S. Vanicek, J. Beerhues, T. Bens, V. Levchenko, K. Wurst, B. Bildstein, M. Tilset, B. Sarkar, *Organometallics* **2019**, *38*, 4383–4386.
[87] M. Pažický, A. Loos, M. J. Ferreira, D. Serra, N. Vinokurov, F. Rominger, C. Jäkel, A. S. K. Hashmi, M. Limbach, *Organometallics* **2010**, *29*, 4448–4458.
[88] P. de Frémont, R. Singh, E. D. Stevens, J. L. Petersen, S. P. Nolan, *Organometallics* **2007**, *26*, 1376–1385.
[89] P. Kühlkamp, H. G. Raubenheimer, J. S. Field, M. Desmet, *J. Organomet. Chem.* **1998**, *552*, 69–74.
[90] STOE & Cie, *X-Area*, STOE & Cie, Darmstadt, Germany.
[91] R. H. Blessing, *Acta Crystallogr. Sect. A* **1995**, *51*, 33–38.
[92] A. L. Spek, *Acta Crystallogr. Sect. D* **2009**, *65*, 148–155.
[93] J. Koziskova, F. Hahn, J. Richter, J. Kožíšek, *Acta Chim. Slov.* **2016**, *9*, 136–140.
[94] G. M. Sheldrick, *Acta Crystallogr. Sect. A* **2015**, *71*, 3–8.
[95] G. M. Sheldrick, *Acta Crystallogr. Sect. C* **2015**, *71*, 3–8.
[96] G. M. Sheldrick, *SHELXL-2018/3*, University of Göttingen, Göttingen, Germany, **2018**.
[97] C. B. Hübschle, G. M. Sheldrick, B. Dittrich, *J. Appl. Crystallogr.* **2011**, *44*, 1281–1284.
[98] F. Neese, *WIREs Comput. Mol. Sci.* **2018**, *8*.
[99] A. D. Becke, *J. Chem. Phys.* **1993**, *98*, 5648–5652.
[100] C. Lee, W. Yang, R. G. Parr, *Phys. Rev. B* **1988**, *37*, 785–789.
[101] B. Miehlich, A. Savin, H. Stoll, H. Preuss, *Chem. Phys. Lett.* **1989**, *157*, 200–206.
[102] A. Schäfer, H. Horn, R. Ahlrichs, *J. Chem. Phys.* **1992**, *97*, 2571–2577.
[103] A. Schäfer, C. Huber, R. Ahlrichs, *J. Chem. Phys.* **1994**, *100*, 5829–5835.
[104] S. Miertuš, E. Scrocco, J. Tomasi, *Chem. Phys.* **1981**, *55*, 117–129.
[105] V. Barone, M. Cossi, *J. Phys. Chem. A* **1998**, *102*, 1995–2001.
[106] D. A. Pantazis, X.-Y. Chen, C. R. Landis, F. Neese, *J. Chem. Theory Comput.* **2008**, *4*, 908–919.
[107] E. van Lenthe, E. J. Baerends, J. G. Snijders, *J. Chem. Phys.* **1993**, *99*, 4597–4610.
[108] C. van Wüllen, *J. Chem. Phys.* **1998**, *109*, 392–399.
[109] F. Neese, F. Wennmohs, A. Hansen, U. Becker, *Chem. Phys.* **2009**, *356*, 98–109.
[110] R. Izsák, F. Neese, *J. Chem. Phys.* **2011**, *135*, 144105.
[111] S. Kossmann, F. Neese, *Chem. Phys. Lett.* **2009**, *481*, 240–243.
[112] S. Grimme, J. Antony, S. Ehrlich, H. Krieg, *J. Chem. Phys.* **2010**, *132*, 154104.
[113] S. Grimme, S. Ehrlich, L. Goerigk, *J. Comput. Chem.* **2011**, *32*, 1456–1465.
[114] G. R. Fulmer, A. J. M. Miller, N. H. Sherden, H. E. Gottlieb, A. Nudelman, B. M. Stoltz, J. E. Bercaw, K. I. Goldberg, *Organometallics* **2010**, *29*, 2176–2179.
[115] K. Škoch, I. Císařová, J. Schulz, U. Siemeling, P. Štěpnička, *Dalton Trans.* **2017**, *46*, 10339–10354.
[116] K. Škoch, I. Císařová, P. Štěpnička, *Chem. Eur. J.* **2018**, *24*, 13788–13791.

Manuscript received: October 19, 2021
Revised manuscript received: November 4, 2021
Accepted manuscript online: November 9, 2021